

STRUCTURAL PHASE EVOLUTION AND DIELECTRIC RESPONSE IN (BiFeO₃) MULTIFERROIC OXIDE

H. ANWAR^a, H. AKHTAR^{*a}, M. U. ASLAM^a, N. AMIN^b, M. R. SALLEM^b,
G. MURTAZA^c, M. ASIF^d, A. ALI^d, M. HUSSAIN^e, G. MUSTAFA^e

^aDepartment of Physics, University of Agriculture Faisalabad, 38040, Pakistan

^bDepartment of Physics, G.C University, Faisalabad 38000, Pakistan

^cDepartment of Physics, G.C.U. FSD. Layyah Campus, Layyah, 31200, Pakistan

^dDepartment of Physics, COMSATS Inst. of Infor. Tech. Lahore, 54000 Pakistan

^eDepartment of Physics, Bahauddin, Zakariya University Multan, 60800, Pakistan

Bismuth ferrite (BFO) was prepared by using the solution evaporation technique. The investigation of structural and dielectrical properties were carried out by using these samples X-ray diffraction (XRD), scanning electron microscope (SEM) and dielectric measurements. The effect of annealing temperature 450-650°C of nanoparticles was studied. XRD revealed the prepared samples have pure phase and crystallite sizes calculated from Debye Scherrer formula lies in the range of 42.6-77.9 nm. The results exhibit the increasing crystallite size with increasing temperature. The results revealed the morphological and dimensional changes in BFO. Permittivity decreases with increasing frequency of following Maxwell Wagner Model. The samples exhibit dielectric constant (65,72 and 108) and low loss tangent (0.8, 1.0 and 1.5) in the frequency range 10Hz to 3MHz. The characterization of the dielectric losses revealed large leakage current which caused by the secondary phase and crystallite size > 62 nm. Furthermore, ac conductivity is explained on the basis of Maxwell-Weigner and Koops model. The results revealed the materials these have potential applications in switching and electronic devices.

(Received October 29, 2017; Accepted March 7, 2018)

Keywords: Bismuth ferrite; Solution Evaporation technique; X-ray diffraction

1. Introduction

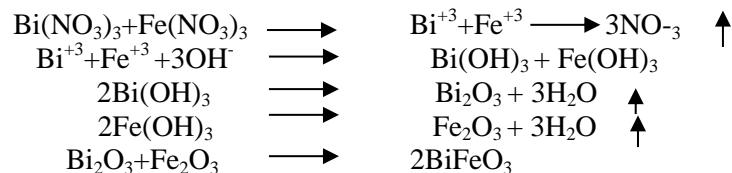
Multiferroics are a class of multifunctional materials which show ferroelectricity, ferromagnetism and ferroelasticity at the same time as a result of the coupled electric, magnetic, mechanical and structural properties [1-2]. As a typical single-phase multiferroic material, perovskite-type BiFeO₃ (BFO) compounds, having a relatively high Neel temperature ($T_N = 643$ K) and Curie temperature i.e. ferroelectric to paraelectric transition temperature at ($T_C = 1143$ K) [3]. In general, bismuth ferrite shows a rhombohedrally deformed perovskite crystal structure with space group R_3C and G-type anti-ferromagnetism at room temperature. BFO has been emerged as one of the suitable materials to comprehend the physics of multiferroic materials that the stereo chemical activity of the Bi ions pair electrons ($6s^2$) which provide ferroelectricity and partially filled 3d orbital of the Fe^{+3} ions cause anti-ferromagnetism [4]. It has attracted to increase the research interest during the past several years, because it could be widely used in micro-electronic devices such as multiple state memory devices, data storage, optical, spintronic devices and sensors [5]. Synthesizing single phase BFO without any secondary or ternary phases (such as Bi₂O₃, Fe₂O₃, Bi₂Fe₄O₉ and Bi₂₅FeO₃₉) is still a difficult task due to different challenges involved in the existing methods. In addition, BFO faces several issues in the primary ferroic properties such as small remanent polarization, large leakage current, high coercive field and weak magneto-electric coupling effects [6-7]. Avoiding impurities is one of the primary concerns regarding the synthesis of such single-phase multiferroic materials; the impurities are caused which arise from three different causes. First, the evaporation of Bi component occurs easily at the onset of

*Corresponding authors: hassanakhtaruaif@gmail.com

synthesis because of low decomposition temperature of bismuth salts; This Bi_2O_3 component appears again in the final production as an impurity. Second, the chemical valence of Fe ions varies in an oxygen-deficient atmosphere; the charge defects with respect to Fe^{+2} ions produced in the synthesis, usually related to the large leakage currents in BFO. Third, the synthesis area of single-phase BFO in the phase diagram of $\text{Bi}_2\text{O}_3\text{-Fe}_2\text{O}_3$ is very narrow from the viewpoint of thermodynamics, in which two kinds of impurities ($\text{Bi}_2\text{Fe}_4\text{O}_9$ and $\text{Bi}_{25}\text{FeO}_{39}$) are usually appeared [8]. In the recent years, many promising methods have been adapted for one thing to overcome these challenges to achieve an extensive material BFO such as; solid-state reaction [9], sol-gel technique [10], Co-precipitation method [11], Glycol gel method [12], Modified Pechini method [13], Microemulsion method [14] and hydrothermal synthesis [15]. During the solid state reaction synthesis of BFO, the kinetics of phase formation in the $\text{Bi}_2\text{O}_3\text{-Fe}_2\text{O}_3$ system can easily lead to the appearance of second phase ($\text{Bi}_{25}\text{FeO}_{40}$, $\text{Bi}_2\text{Fe}_4\text{O}_9$), which need to be removed by using diluted nitric acid [9]. For instance, the sol-gel method is able to substantially lower synthesis temperature $300\text{-}500^\circ\text{C}$, reducing impurities with a great extent. Using an oxygen-enriching atmosphere can keep the Fe ion in Fe^{+3} form, which minimizes the leakage current of BFO [10]. In co-precipitation method, prepared a nanosized BFO powders, the excess Bi content can effectively compensate for the evaporation of Bi component in the chemical reaction during the calcinations process [11]. Glycol gel method obtained conventional secondary phase in the doped BFO under these parameters drying -80°C , calcinations 450°C , and sintering temperature (800°C) and quenching [12]. According to Kumra et al [13] solvents such as HNO_3 and ethanol chelating agents such as citric acid and tartaric acid, polymerizing agents such as ethylene glycol, drying 100°C , calcinations 600°C , and sintering temperature 800°C and observed secondary phases $\text{Bi}_{36}(\text{Bi}_{0.5}\text{Fe}_{0.5}\text{O}_{19.5})$. Nandini das et al reported [14] synthesized phase pure nanosized BFO powders by microemulsion techniques in the temperature range of $400\text{-}500^\circ\text{C}$. The sol-gel hydrothermal processing represents an alternative to the calcinations for the crystallization of an objective compound under mild temperatures. Solvent such as H_2O mineralizes such as KOH and NaOH, solvent temperature 200°C . Hydrothermal technique has advantages due to its high degree of crystallinity, well-controlled morphology, high purity, and narrow particle size distribution of the prepared powders [15]. It is evident that the hydrothermal environment remarkable accelerates the kinetics of the formation of BiFeO_3 . All these existing methods require subtle parameters such as processing temperature, pressure, time and various temperature treatment steps such as drying, calcinations and sintering. Similarly, these methods require different solvents and chelating agents, polymerizing agents, etc. which are to be effectively optimized to synthesis the single phase, impurity free BFO ceramics and nanopowders. In this study, a simple solution evaporation technique is proposed by synthesis of pure single-phase BiFeO_3 powders. The production of impurities can be avoiding by controlling the technical parameters using the law of thermodynamics as bases. Also investigates the phase and morphology evolutions of BFO with respect to the different annealing temperature and collectively discusses their influence on the structural and dielectric properties of multiferroic material BFO.

2. Experimental procedure and Instrumentation

The raw materials used in the present work are analytical grade bismuth nitrate pentahydrate $\text{Bi}(\text{NO}_3)_3 \cdot 5\text{H}_2\text{O}$ and iron nitrate nonahydrate $\text{Fe}(\text{NO}_3)_3 \cdot 9\text{H}_2\text{O}$. (BFO) precursor, the reactant Fe_2O_3 and Bi_2O_3 were in stoichiometric proportion and dissolved in deionized water. Add 2 ml of nitric acid to get homogenous mixture in it, which placed it on hot plate for evaporation and heated the solution at temperature 160°C under constant stirring until all the liquid evaporated. The formation kinetics of BFO nanoparticles as under blew process:



The dry precipitates were mixed homogeneously with the help of an agate mortar and pestle for 30 min. Paul-Otto Weber Hydraulic Press pelletizes the obtained powder under the load of 60KN for 3 min. The pellets (6mm x2mm) and the powder was sintered at 450 °C, 550 °C and 650 °C for 2 h in a box furnace and was slowly cooled down to room temperature to yield the final product. The X-ray diffraction (XRD) patterns were obtained at room temperature using powder samples in an Xpert Pro PANalytical diffractometer with Cu-K α radiation ($\lambda = 1.54056 \text{ \AA}$) at 40 kV and 30 mA. The intensity have been collected by the step counting method (with a scanning speed 0.05°/s) in the 2 θ range from 20° -70°. The surface morphology and microstructure of the samples were studied by JSM-6490 JEOL scanning electron microscope (SEM). The dielectric properties of multiferroic materials were measured at room temperature by using Wayn Ker WK-6500B instrument.

3. Results and discussion

3.1. Structural Analysis

The XRD patterns of BFO powders synthesized at 160 °C for 12 h by solution evaporation technique. The synthesized powders calcined at different temperatures at 450 °C, 550 °C and 650 °C for 2 h for investigation of structural evolution of multiferric material. All the reflection peaks in these XRD patterns which can be indexed to perovskite (space group R3c) BiFeO₃ and found conventional secondary phase were detected. The X-ray diffraction data measured through reitveld refinement method by using GSAS software. The impurity peaks which has been observed at different angles like 2 $\theta = 25.8^\circ$, 29.3° and 34.2° as shown in Fig. 1. Bismuth ferrite peaks were observed at (012), (104), (202) and (024) plane having 2 θ at 23.2°, 32.6°, 38.8° and 47.9° respectively. The crystallite size measured all the samples by Scherrer's formula:

$$D = \frac{k \lambda}{B_{(hkl)} \cos \theta} \quad (1)$$

Where K is the shape factor, λ is the X-ray wavelength and θ is the Bragg's diffraction angle. The crystallite size of the synthesized materials was found 42.6 nm 450 °C, 47.8 nm 550 °C and 77.9 nm 650°C respectively. The growing crystalline size observed by the growth of the material intensity and sharpening of peaks depended on heat treatment. The trend of crystallite size as shown in Fig. 2

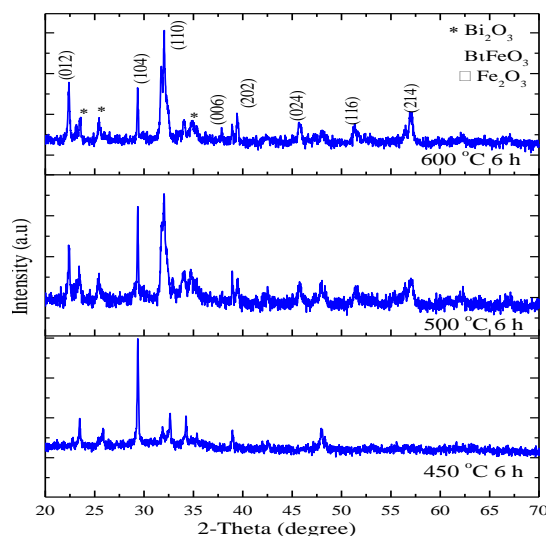


Fig.1 X-ray diffraction pattern of BFO annealed at (a) 450°C (b) 550°C and (c) 650 °C.

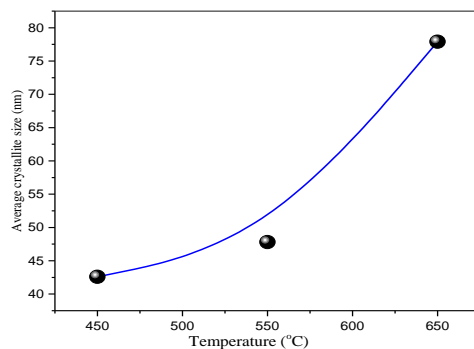


Fig. 2 Annealing temperature versus average crystallite size (nm)

3.3 Scanning Electron Microscope Analysis

Fig.3 (a-d) shows the (SEM) images of the BFO samples synthesized by solution evaporation method at different temperatures at 450 °C, 550 °C and 650 °C for 2 h respectively. It can be seen, the products show different microstructure like spherical microstructure, rectangular shape and agglomerated with irregular morphology. Generally, such interesting morphologies are produced in the hydrothermal synthesis. This type of anisotropic dendrites like growth of particles is possible in this hydrothermal technique due to diffusivity between the two-phase compounds (Bi_2O_3 , Fe_2O_3). Hence, the BFO show spherical agglomerate likes structure, due to the exaggerated particle growth, when the annealing temperature is 650°C. This type of phenomenon is common in oxides, ferrites and titanate materials. In general, the anisotropic growth of particles is due to: (1) Materials with high chemical equilibrium. (2) Materials with high anisotropy in interfacial energy. (3) Secondary phases or impurities. (4) Weak Van der wall bonds and magnetic forces may play the role to cling to these agglomerations. (5) The careful study of the images suggests that the bismuth ferrite grains are well packed but non uniform distribution of grain sizes exists.

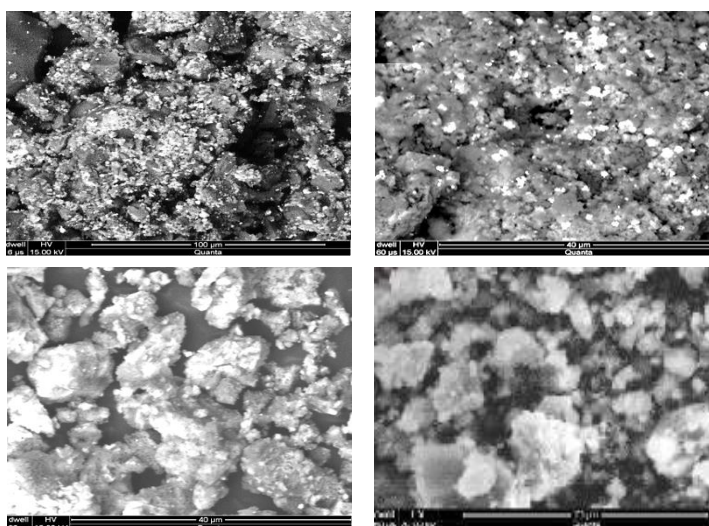


Fig.3 SEM image of (BFO) annealed at (a) 450°C (b) 550 °C and (c-d)650°C for 2 h.

For the purposes of warm absorption, such typical shapes are favorable. The difference in grain size is because grains are composed of several particles, which may introduce the internal stress or defects in the structure.

3.3. Dielectric properties

In order to measure the dielectric properties the impedance analyzer HIOKI 3532 LCR HITESTER covered a range of 10Hz to 3 MHz. It was used to measure the complex dielectric properties of the synthesized materials. For the measurement, a pellet of thickness 1.5 mm was painted with silver paste on both sides and then fired at 200 °C for 10 minutes. In the present study, the measurement of capacitance was performed at room temperature while the dielectric constant (ϵ') and loss tangent ($\tan \delta$) were obtained using the recorded data. The samples of ferromagnetic materials made in the form of capacitor are electrically equivalent to the combination of capacitor C_p and resistor R_p , both connected in a parallel combination. Impedance analyzer measured the values of the capacitance and resistance, while the dielectric properties were calculated using the following formulae [16-17].

$$\epsilon' = \frac{C_o}{C_p} \quad \text{where } C_o = \frac{A \epsilon_0}{d} \quad (2)$$

$$\tan \delta = \frac{1}{\omega C_p R_p} \quad (3)$$

$$\rho_{ac} = 2\pi f \epsilon_0 \epsilon' \tan \delta \quad (4)$$

3.4.1. Frequency dependent dielectric constant

The dielectric constant (ϵ') which have high value of dielectric constant at lower frequency is due to space charge polarization. The dielectric constant and loss become almost frequency independent at high frequency; this indicates the rotational motion of the polar molecules of the dielectric is not sufficiently rapid for the attainment of equilibrium with the field. The dielectric constant behavior of the sample in the frequency range (10 Hz to 3 MHz) can be observed in Fig.4. On increasing the frequency, the dielectric constant is found to decrease monotonously and it approaches a constant value at higher frequency. The dielectric constant probably results from the rapid polarization processes occurring in the materials at low frequency. The high value of the dielectric constant at low frequency is as expected due to increased contribution of different types of polarizations, i.e., dipole, atomic, ionic, electronic and interfacial [18-19]. However, the dielectric behavior can be inferred from Maxwell-Wagner interfacial type polarization [20].

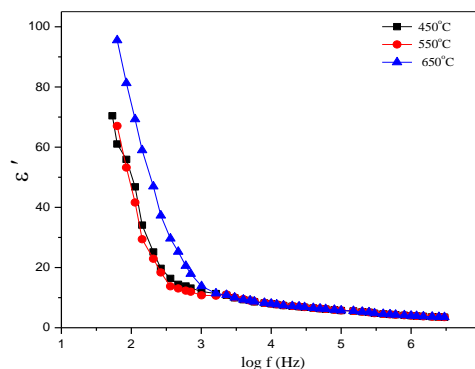


Fig. 4 Dielectric constant as a function of log of frequency for BFO nanoparticles

3.4.2. Dielectric Tangent Loss ($\tan \delta$)

The ratio between the loss current and the charging current in a material is called tangent loss. The tangent loss plot is shown in the Fig.5 which shows that the tangent loss is almost invariant with the increasing of frequency from 10Hz to 3MHz.

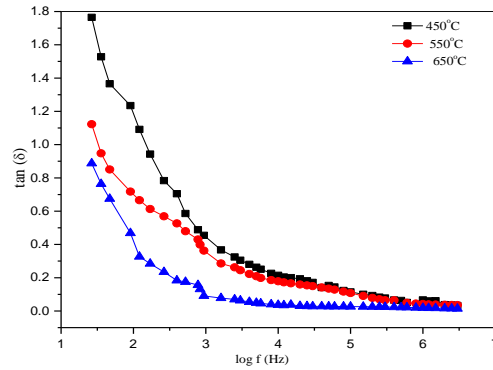


Fig. 5 Dielectric loss ($\tan \delta$) as a function of log of frequency

3.4.3 AC-Conductivity

The total conductivity, generally the AC conductivity, of semiconducting nature of ferrites analysis with two terms that can be written as follows:

$$\sigma_{(\omega, T)} = \sigma_1(T) + \sigma_2(\omega, T) \quad (5)$$

Where the first term $\sigma_1(T)$ is the DC part of the electrical conductivity that follows an Arrhenius relation and it is related to the drift mobility of free charge carriers. The second term $\sigma_2(\omega, T)$ is frequency and temperature dependent that is related to the dielectric relaxation due to the localized electric charge carriers and obeys the power law.

$$\sigma_2(\omega, T) = A(\omega)^n \quad (6)$$

where $\omega = 2\pi f$, is the angular frequency of applied voltage. It has conductivity units $(\Omega\text{cm})^{-1}$. The exponent parameter 'n', a non-dimensional temperature dependent parameter, has values between 0 and 1 which provides the information about the properties of the material and increases with increase of ion-ion interaction [21]. The ac conductivity shows an increasing trend at low frequency region however at higher range of frequencies it exhibits the dispersion behavior. It is inferred that attitude of ac conductivity at low frequencies depends upon the behavior of the grain boundary, while the dispersion at high frequency may be attributed to the conductivity of grains [22].

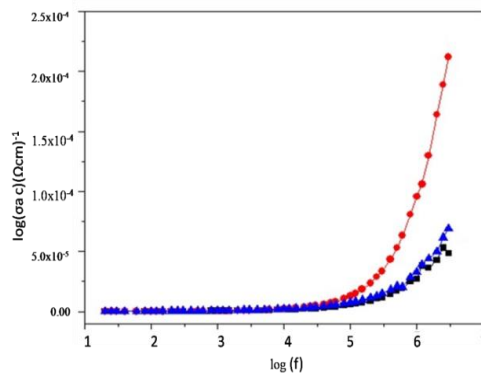


Fig.6 Variation of ac conductivity (σ_{ac}) with log frequency for BFO

Fig.6 shows a plot between $\log(\sigma)$ versus $\log(\omega)$ in which ac conductivity increases with the increase of frequency of applied field. Since the increase in frequency enhances the hopping frequency of the charge carriers between Fe^{2+} and Fe^{3+} , so the conductivity increases. These results revealed that the large leakage current which caused by the secondary phase and bigger crystallite size 77.9 nm.

4. Conclusions

A simple method was used to prepare pure BFO nanopowders at different annealing temperature (450-650°C). The stability of the perovskite phase increases at high temperature. A longer annealing temperature was beneficial to inhibit the formation of any impurity phase and prompted the growth of BFO crystallites into single-phase perovskites. It was found that crystallite size lies in the range which measured by Scherrer's formula (42.6-77.9 nm). Scanning electron microscopy (SEM) images showed morphological distribution of grain size, and dimensional changes in BFO. The dispersion of ac conductivity is explained based on Maxwell-Weigner and Koops model. The increase in ac conductivity was due to the creation of additional hopping sites in the material. It is concluded from these properties, the material may be suitable for the application of electronic devices.

Acknowledgements

The author (G.Mustafa) is thankful to the Higher Education Commission (HEC) of Pakistan for the financial assistance under HEC Indigenous Scheme and International Research Support Initiative Program (IRSIP).

References

- [1] W. Eerestein, N. D. Mathur, J. F. Scott, *Nature* **442**, 759 (2006).
- [2] T. J. Park, G. C. Papaefthymiou, A. J. Viescas, A. R. Moodenbaugh, S. S. Wong, *NanoLett.* **7**, 766 (2007).
- [3] J. Dho, X. Qi, H. Kim, J. L. MacManus-Driscoll, M.G. Blamire, *Adv. Mater.* **18**, 1445 (2006).
- [4] V. A. Khomchenko et al, *J. Magn. Magn. mater.* **321**, 1692 (2009).
- [5] J. Wang, J. B. Neaton, H. Zheng, V. Nagarajan, S. B. Ogale, B. Liu, D. Viehland, V. Vaithyanathan, D. G. Schlom, *Science* **299**, 1719 (2003)
- [6] K. L. Yadav, *J. Nanosci, Nanotechnol.* **11**, 4097 (2011).
- [7] H. Yang, T. Xian, Z. Q. Wei, J. F. Dai, J. L. Jiang, W. J. Feng, *J. Sol. gel. Sci. Tech.*, **58**, 238 (211).
- [8] J. Yu, N. Koshikawa, Y. Arai, S. Yoda, H. Saitou, *J. Cryst. Growth.* **231**, 568 (2001).
- [9] M. Valant, A. K. Axelsson, N. Alford, *Chem. of Mater.* **19**, 5431 (2007).
- [10] Z. Chen, G. Zhan, X. He, H. Yang, H. Wu, *Cryst. Res. Tech.* **46**(3), 309 (2011).
- [11] H. Ke, W. Wang, Y. Wang, J. X. D. Jia, Z. Lu, Y. Zhou, *J. Alloy. Comp.* **509**, 2192 (2011).
- [12] Q. Xu, H. Zai, D. Wu, Y. K. Tang, M. X. Xu, *J. Allows. Compd.* **485**, 13 (2009).
- [13] M. Kumra, K. L. Yadav, G. D. Varma, *Mater. Lett.* **62**, 1159 (2008).
- [14] N. Das, R. Majumdar, A. Sen, H. S. Maiti. *Mater. Lett.* **61**, 2100 (2007).
- [15] Y. P. Wang, L. Zhou, M. F. Zhang, X. Y. Chen, J. M. Liu, Z. G. Liu, *Appl. Phys. Letter.* **84**, 1731 (2004).
- [16] M. M. Kumar, V. R. Palkar, *Appl. Phys. Lett.* **76**, 2764 (2000).
- [17] G. L. Yuan, K. Z. Baba-Kishi, J. Liu, Y. P. Wang, Z. G. Liu, *J. Am. Ceram. Soc.* **89**, 3136 (2006).
- [18] V. R. Palkar, D. C. Kundaliya, S. K. Malik, *J. Appl. Phys.* **93**, 4337 (2003).
- [19] V. A. Khomchenko, D. A. Kisolev, J. M. Vieira, A. L. Kholkin, M. A. Sa, Y. G. Pogorelov, *Appl. Phys. Lett.* **90**, 242901 (2007).

- [20] V. A. Khomchenko, D. A. Kiselev, J. M. Vieira, J. Li, A. L. Kholkin, A. M. L. Lopes, Y. G. Pogorelov, J. P. Araujo, M. Maglione, *J. Appl. Phys.* **103**, 024105 (2008).
- [21] V. B. Naik, R. Mahendiran, *Solid State Communications* **149**, 754 (2009).
- [22] R. D. Shannon, *Acta Cryst. A* **32**, 751 (1976).